ACS APPLIED MATERIALS & INTERFACES

Research Article

www.acsami.org

Optical and Conductive Properties of As-Synthesized Organic-Capped TiO_2 Nanorods Highly Dispersible in Polystyrene-*block*-poly(methyl methacrylate) Diblock Copolymer

Laida Cano,[†] Angela Evelyn Di Mauro,[‡] Marinella Striccoli,[‡] M. Lucia Curri,[‡] and Agnieszka Tercjak*[,†]

[†]Group Materials and Technologies, Chemical Engineering and Environmental Department, Polytechnic School, University of the Basque Country (UPV/EHU), Plaza Europa 1, 20018 Donostia−San Sebastián, Spain

[‡]CNR-IPCF Bari Division, Chemistry Department, University of Bari, Via Orabona 4, 70126 Bari, Italy

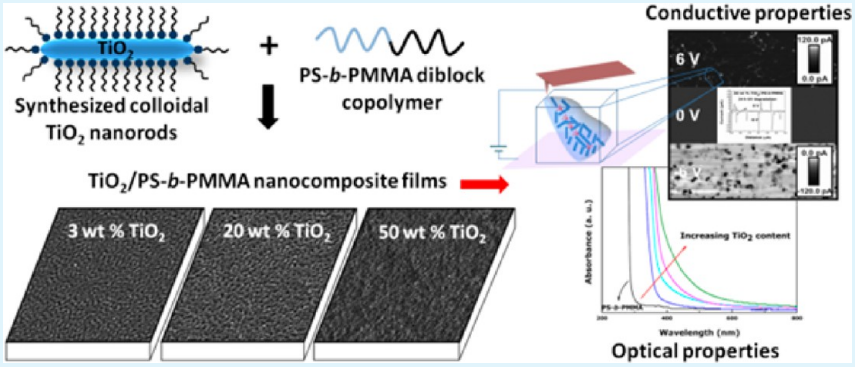

ABSTRACT: As-synthesized organic-capped TiO_2 nanorods were incorporated into polystyrene-*block*-poly(methyl methacrylate) (PS-*b*-PMMA) diblock copolymer to achieve TiO_2/PS-*b*-PMMA nanocomposites with enhanced optical and conductive properties. The specific surface chemistry of TiO_2 nanorods derived from the colloidal synthetic approach allowed their prompt incorporation in the PS-*b*-PMMA block copolymer template up to 50 wt %, which resulted in films with an extended coverage of highly dispersed nanoparticles for contents higher than 30 wt %. At such high nanorod contents, the films fabricated by the prepared nanocomposites demonstrated enhanced optical properties. Atomic force microscopy investigation of the nanocomposite films showed a cylindrical morphology for low nanorod contents. Conversely, higher nanorod contents resulted upon removal of the organic component in the nanocomposites with UV treatment in overall nanorod coverage of the film surface with the concomitant formation of charge percolation paths, which led to noticeable conductivity values. EFM and PF-TUNA measurements confirmed the conductive properties of the composites at nanoscale, whereas semiconductor analyzer measurements provided their macroscale characterization. In addition, an increase in the UV−vis absorption was observed with the increase in the nanorod content along with a remarkable conductivity of the overall film.

KEYWORDS: *PS-b-PMMA, self-assembled block copolymers, colloidal TiO_2 nanorods, AFM, TUNA, EFM*

INTRODUCTION

Hybrid materials composed of a polymeric matrix and an additive with the characteristic length in the nanometer scale are currently one of the most studied areas in the field of polymer composites.[1−7] In general, the properties of a composite created by combining two or more materials mainly depend on the properties of the constituent components. In the particular case of nanocomposites, where at least one component belongs to the nanoscale, the addition of a nanofiller such as nanoparticles, carbon nanotubes, nanofibers, or cellulose nanocrystals, among others, can have a strong effect on the properties of the resulting material due to the small size of the filler compared to more conventional ones and, consequently, to the component's original and size-dependent characteristics, including surface area. The peculiar features of nanomaterials make them very interesting. Even when added in a low proportion to the composite matrix, nanomaterials can achieve a much more significant enhancement of a specific property than that observed with the use of a material of larger dimension. Namely, nanofillers can significantly improve different properties of the materials into which they are incorporated, such as optical, electrical, mechanical, or thermal properties.[2−4,7−11]

The improvement of these properties is dependent on the microstructure of the nanocomposite. In this regard, the morphological control of nanocomposites has recently gained increasing attention. Among the different methods used to obtain nanostructured nanocomposites with controlled morphology, one of the most employed strategies relies on the use of block copolymers as matrices in nanocomposites. Block

Received: April 29, 2014
Accepted: June 30, 2014
Published: June 30, 2014

copolymers are ideal materials for this purpose because chemically different blocks are covalently linked each other, thus resulting in structures that are able to self-assemble into a rich variety of ordered nanoscale morphologies. This ordering can be achieved not only by self-assembly but also by the application of external fields, such as solvent vapor annealing,[12,13] mechanical flow,[14,15] or electrical field,[16] among others, that induce an enhanced morphology alignment of the block copolymers. Consequently, block copolymers can be ideal scaffolds or templates to pattern nanoparticles[17−23] or for the fabrication of hybrid structures to be integrated in devices for various electronic, optical, and optoelectronic applications.

Nanoparticles incorporated into a block copolymer matrix can significantly affect a wide range of the material properties. However, the enhancement of such properties generally depends on the kind of nanoparticle dispersion in the block copolymer matrix and, in particular, on the ability to control the nanoparticle localization within the host matrix. Many studies have reported diverse procedures to somehow direct the nanoparticles into a specific phase of a block copolymer, and it has been widely proved that the use of block copolymers is a simple way to achieve the desired positioning of nanoparticles in the polymeric matrices determined by the morphology achieved by block copolymer self-assembly.[17−20]

Generally, two main approaches can be followed to prepare nanoparticles/block copolymer nanocomposites as a function of the nanoparticle synthetic protocol.[19] The first one is based on an in situ synthesis of the inorganic nanoparticles within a block copolymer domain. In the second case, the synthesis of nanoparticles is accomplished ex situ before their incorporation in the block copolymer. In the latter case, the surface functionalization of the nanoparticles can be tuned to achieve preferential confinement of nanoparticles in a specific block copolymer domain. In addition, such an approach allows a careful and precise control of the nanoparticle size and shape, and, accordingly, of their size-dependent properties, along with a suitable tailoring of the nanoparticle surface chemistry. In particular, surface functionalization is responsible for the chemical affinity between nanoparticles and one block of the block copolymer; therefore, this can be exploited to direct the nanoparticles into the target block copolymer domain during the assembling process. Here, ex situ synthesized nanoparticles have been incorporated into a block copolymer, and the obtained nanocomposites have been allowed to self-assemble.

Inorganic nanoparticles and nanocrystals are characterized by original chemical and physical size- and shape-dependent properties, which strongly differ from those observed in the corresponding bulk counterparts. Among the different types of nanomaterials, semiconducting titanium dioxide (TiO_2) nanoparticles have attracted attention, owing to their several potential applications in fields such as photocatalysts, sensors, solar cells, and memory devices.[24,25]

Recently, many studies have reported the fabrication of hybrid nanocomposites based on a block copolymer acting as template for the incorporation of TiO_2 nanoparticles.[26−34] Most investigations report the in situ method for the synthesis of TiO_2 nanoparticles carried out by means of sol−gel technique inside the block copolymer solution,[27−31,33] while other examples account for the ex situ TiO_2 nanoparticles synthesis prior to incorporation into a block copolymer.[26,32] In our work, semiconductor TiO_2 colloidal nanorods have been obtained ex situ by means of a colloidal chemistry procedure,[35−38] which enabled us to control their size and shape. Oleic acid has been used as a surfactant to control nanorod growth during the synthesis, and coordinating the nanorod surface prevents their aggregation and allows them to disperse in an organic apolar environment. Therefore, prompt processing of the obtained organic-coated nanorods has been achieved. In particular, nanorods have been effectively dispersed in toluene and then incorporated in polystyrene-*block*-poly(methyl methacrylate) (PS-*b*-PMMA) diblock copolymer, which is used as a template. The most important factor for achieving an affective confinement of nanoparticles in one phase of the block copolymer is the compatibility between nanoparticles and one block of the block copolymer, which, in this case, has been achieved due to the organic capping layer of the nanoparticles. Optical properties of nanocomposite solutions have been investigated by means of UV−vis absorption spectroscopy. Nanocomposites, with the increase of nanorod content, have then been deposited as thin film by spin-coating and characterized by atomic force microscopy (AFM) to study the morphologies of the different TiO_2/PS-*b*-PMMA nanocomposites as well as the dispersion and positioning of the incorporated nanorods within PS-*b*-PMMA block copolymer. Conductive properties of nanocomposite films have been analyzed at nanoscale by electrostatic force microscopy (EFM) and PeakForce tunneling atomic force microscopy (PF-TUNA), while a semiconductor analyzer has been used for electrical investigation at macroscale.

EXPERIMENTAL SECTION

Materials. Polystyrene-*block*-poly(methyl methacrylate) (PS-*b*-PMMA) diblock copolymer used as template to disperse TiO_2 nanorods was purchased from Polymer Source, Inc. with a polydispersity index (M_w/M_n) of 1.17 and number-average molecular weights of PS and PMMA blocks of 83 000 and 92 500 g/mol, respectively. For the synthesis of TiO_2 nanorods, titanium tetraisopropoxide ($Ti(OPri)_4$ or TTIP, 99.999%), trimethylamino-*N*-oxide dihydrate ($(CH_3)_3NO\ 2H_2O$ or TMAO, 98%), and oleic acid ($C_{18}H_{33}CO_2H$ or OLEA, 90%) were purchased from Aldrich. Toluene and methanol were purchased from Aldrich. Toluene for the nanocomposite preparation was supplied by Labscan and used as solvent.

Synthesis of TiO_2 Nanorods. The synthesis of TiO_2 nanorods was performed by following a previously reported method.[37,39] Briefly, TTIP was added to previously degassed OLEA under nitrogen flow at 100 °C. Subsequently, an aqueous solution of TMAO was rapidly injected, which started the fast hydrolysis, leading to the formation of OLEA-coated anatase TiO_2 nanorods (average size: 3 nm in diameter, 18 nm in length). The obtained nanorods were precipitated from the reaction mixture upon the addition of methanol, isolated by centrifugation, and redispersed in toluene. A detailed structural and morphological characterization of the as-prepared OLEA-coated crystalline TiO_2 nanorods can be found elsewhere.[37,39]

Preparation of TiO_2/PS-*b*-PMMA Nanocomposites. First, PS-*b*-PMMA diblock copolymer solutions were prepared by dissolving a defined amount of block copolymer in toluene to reach a concentration of 5 mg/mL. The solution was stirred with a magnet until a homogeneous mixture was obtained. Then, an adequate volume of TiO_2 nanorod solution in toluene was added to block copolymer solution in order to obtain TiO_2/PS-*b*-PMMA nanocomposites with different TiO_2 nanorod content (in the range of 1−50 wt %). Nanocomposite solutions were stirred for a few hours. Both neat block copolymer and nanocomposites were prepared as thin films by spin-coating the corresponding solution (spin coater model P6700 from Specialty Coating Systems, Inc.) onto previously cleaned silicon wafer substrates at 2000 rpm for 120 s. All films were kept at ambient conditions.

Techniques. Fourier transform infrared spectroscopy (FTIR) of oleic acid-coated TiO_2 nanorods in toluene solution was performed by

a Varian 670-IR spectrometer equipped with a deuterated triglycine sulfate detector in attenuated total reflection (ATR) sampling mode. The internal reflection element was a one-bounce 2 mm diameter diamond microprism. Cast films were prepared directly onto the internal reflection element by depositing the solution (3−5 μL) on the upper face of the diamond crystal and allowing the solvent to evaporate completely. The spectral resolution was 4 cm^{-1}.

UV−vis absorption spectra of the solutions of neat PS-*b*-PMMA diblock copolymer and TiO_2/PS-*b*-PMMA nanocomposites in toluene were obtained using a spectrophotometer (Shimadzu UV-3600) in the range between 200 and 800 nm.

The morphologies of films prepared from PS-*b*-PMMA block copolymer and its nanocomposites with TiO_2 nanorods were studied by AFM under ambient conditions using the thin films prepared by spin-coating. AFM measurement was performed using a Dimension Icon scanning probe microscope equipped with Nanoscope V controller (Bruker). Tapping mode (TM) was employed in air using an integrated tip/cantilever (125 μm in length with ca. 300 kHz resonant frequency). Typical scan rates during recording were 0.9−1.1 line/s using a hybrid scan head with a maximum range of 100 × 100 μm.

Conductive properties of TiO_2/PS-*b*-PMMA nanocomposites were investigated by electrostatic force microscopy (EFM). EFM measurements were performed using the same Dimension Icon scanning probe microscope operating in the lift mode (lift height was ∼100−150 nm) in ambient conditions and equipped with a Pt/Ir coating tip with a resonance frequency around 75 kHz. The secondary imaging mode derived from the tapping mode that measures the electric field gradient distribution above the sample surface was detected by applying a voltage to the cantilever tip. This method enabled us to characterize conductive properties at the nanometric level.

Quantitative nanoelectrical properties of the investigated materials were measured using TUNA with the same Dimension Icon scanning probe microscope. The measurements were carried out using PF-TUNA mode under ambient conditions. The PF-TUNA probe was equipped with the same Pt/Ir coating tip used for EFM measurement. The conductive properties of the TiO_2/PS-*b*-PMMA nanocomposites were taken into account, and the quantitative PF-TUNA measurements were performed on the nanocomposites with high nanorod contents and, in order to enhance conductivity in these samples, the organic component of the system was removed by exposing the samples to 254 nm UV light (XX-15S, UVP Inc.) for 24 h.

A semiconductor characterization system (Keithley model 4200-SCS) was used to study the conductive properties of the investigated TiO_2/PS-*b*-PMMA nanocomposites. Two-point experiments were carried out, and we applied a voltage sweep from −4 to 4 V to study the conductive properties at the macroscopic level.

RESULTS AND DISCUSSION

The surface chemistry of TiO_2 nanorods dispersed in toluene was investigated by FTIR spectroscopy. The FTIR spectrum of oleic acid-coated TiO_2 nanorods, shown in Figure 1, exhibited specific signals corresponding to the oleic acid bands. In particular, the TiO_2 nanorod sample showed intense peaks at 2922 and 2850 cm^{-1} attributable to the symmetric and antisymmetric C−H stretching vibrations of the $-CH_2-$ groups in the oleic acid alkyl chain, respectively.

In addition, the spectrum showed a shoulder at approximately 2960 cm^{-1} due to the asymmetric stretching of the terminal $-CH_3$ group of the alkyl chain and the signal at 3005 cm^{-1} that is characteristic of the olefinic C−H symmetric stretching.[40] Below 2000 cm^{-1}, two intense bands centered at 1521 and 1436 cm^{-1} dominated the spectrum due to the COO− antisymmetric and symmetric stretching vibrations, respectively, of carboxylate anions complexed with surface metal centers. On the basis of the frequency difference between these two bands ($\Delta\nu \approx 85$ cm^{-1}), the mode of binding of the

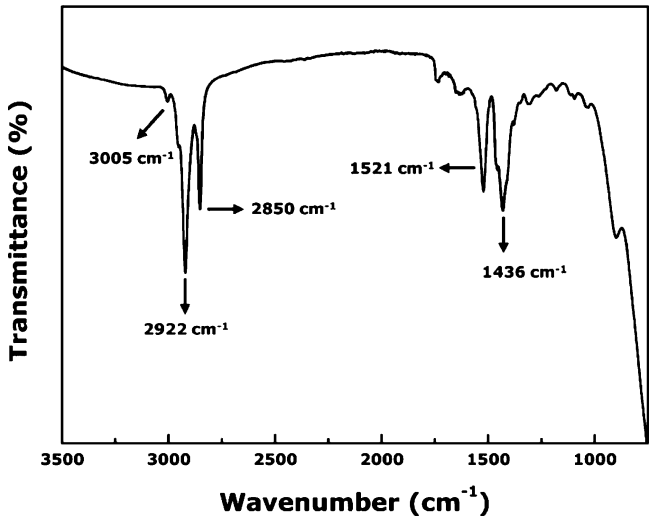

Figure 1. FTIR spectrum of oleic acid-coated TiO_2 nanorods.

carboxylate adsorbates onto the TiO_2 surface can be assigned as predominantly chelating bidentate.[39,40] The characteristic vibrations of the metal−oxygen bonds, below 800 cm^{-1}, were observable in the TiO_2 nanorod samples.[40]

PS-*b*-PMMA block copolymer and TiO_2/PS-*b*-PMMA nanocomposite toluene solutions were investigated via UV−vis absorption spectroscopy. Figure 2 shows the spectrum of neat

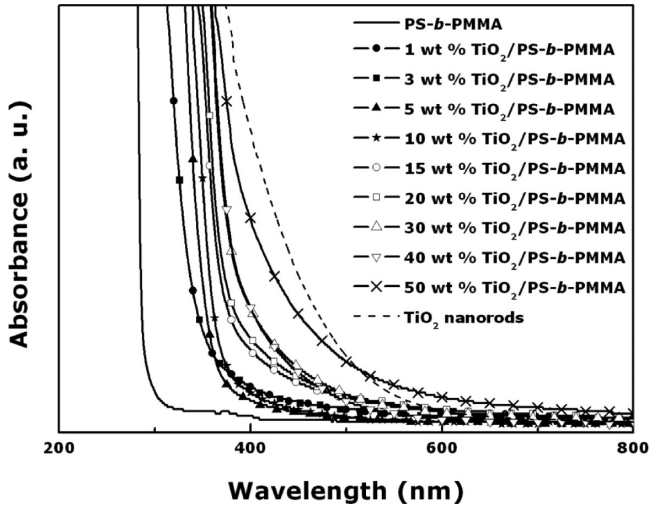

Figure 2. UV−vis absorption spectra of neat PS-*b*-PMMA block copolymer and TiO_2/PS-*b*-PMMA nanocomposites.

PS-*b*-PMMA block copolymer solution, which was characterized by an intense absorption in the UV region below 300 nm. For the spectra of TiO_2/PS-*b*-PMMA nanocomposites, when the nanorod loading was increased, the absorption onset started at a higher wavelength, namely, between 350 and 500 nm, than that of the neat block copolymer,[34,41] with a concomitant broadening of the absorption tail at low energy. Such evidence of absorption onset starting from 350 nm can be definitely accounted for by the presence of the nanosized TiO_2, which, as can be seen in its absorption curve, has a characteristic UV spectrum within a spectral range that defines its UV shielding properties.[42−44] Consequently, the addition of TiO_2 nanorods provided the nanocomposites with UV shielding properties as a function of nanorod content. The

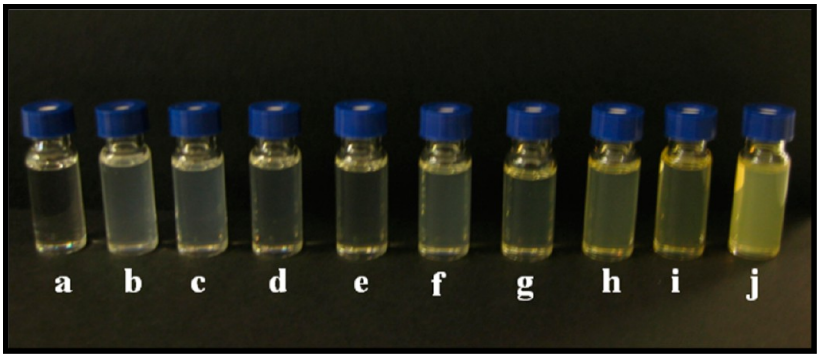

Figure 3. Visual appearance of (a) neat PS-*b*-PMMA block copolymer, (b) 1, (c) 3, (d) 5, (e) 10, (f) 15, (g) 20, (h) 30, (i) 40 and (j) 50 wt % TiO_2/PS-*b*-PMMA nanocomposites.

absorption tail detected in the visible region of the nanocomposite absorption curves can be ascribed to scattering losses induced by the large amount of nanorods dispersed in block copolymer,[36] which is further supported by the increasing extent of the shoulder at higher loading.

All samples, including the neat PS-*b*-PMMA block copolymer and TiO_2/PS-*b*-PMMA nanocomposite toluene solutions, were transparent, although their visual appearance changed with the addition of TiO_2 nanoparticles (Figure 3). Thus, samples up to 10 wt % of TiO_2 nanoparticles were whitish, whereas when more than 10 wt % of TiO_2 nanoparticles was added, the solutions became yellowish.

The morphologies of neat PS-*b*-PMMA block copolymer film and the TiO_2/PS-*b*-PMMA nanocomposites were investigated by AFM. Height and phase AFM images of neat PS-*b*-PMMA block copolymer are shown in Figure 4. The block copolymer film showed a cylindrical morphology with bright microseparated cylinders in a darker matrix. The bright separated cylinders with a diameter of around 30 nm were predominantly in a parallel orientation with respect to the surface, and they corresponded to the PMMA block,[45] on the basis of the contrast in the modulus and viscoelastic behavior between PS and PMMA blocks[46−48] and the fact that the brighter regions in the phase image are related to the phase with higher modulus. In addition to this, after applying the Hoftyzer and van Krevelen method[49] to calculate the Flory−Huggins interaction parameters between toluene as solvent and each block of the block copolymer ($\chi_{PS\text{-}tol}$ = 0.36 and $\chi_{PMMA\text{-}tol}$ = 0.55),[47,50,51] a stronger interaction between PS block and toluene can be expected with respect to that between PMMA block and toluene. Therefore, PS block phase will probably appear as the dark matrix as a consequence of the effect of its stronger affinity with the used solvent.

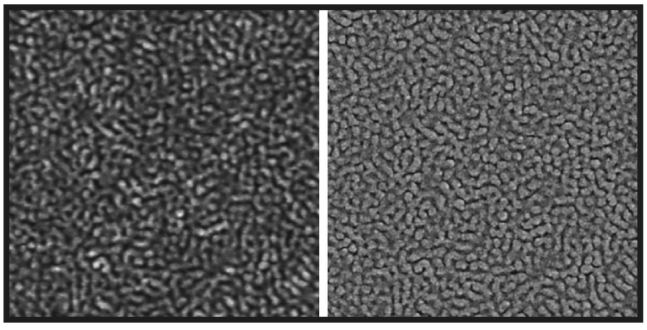

Figure 4. TM-AFM images (2 × 2 μm) of neat PS-*b*-PMMA block copolymer (left) height and (right) phase.

Phase images of all TiO_2/PS-*b*-PMMA nanocomposites with different TiO_2 nanorod contents (1, 3, 5, 10, 15, 20, 30, 40, and 50 wt %) are shown in Figures 5−7. The content of TiO_2 nanorods in the nanocomposites significantly affected the morphology of the final nanocomposite films. The thin films containing up to 10 wt % TiO_2 nanorods (Figures 5 and 6a) maintained the same morphology of the neat block copolymer. In the case of 1 wt % of TiO_2/PS-*b*-PMMA, the morphology was very similar to that of the neat block copolymer with slightly shorter cylinders of PMMA block rich phase. TiO_2 nanorods, which appeared as bright spots in the phase image due to their hardness in comparison to polymeric materials, were rather uniformly dispersed and located mainly in the dark phase corresponding to the PS block, although they were always close to the interphase[52−54] between this phase and the

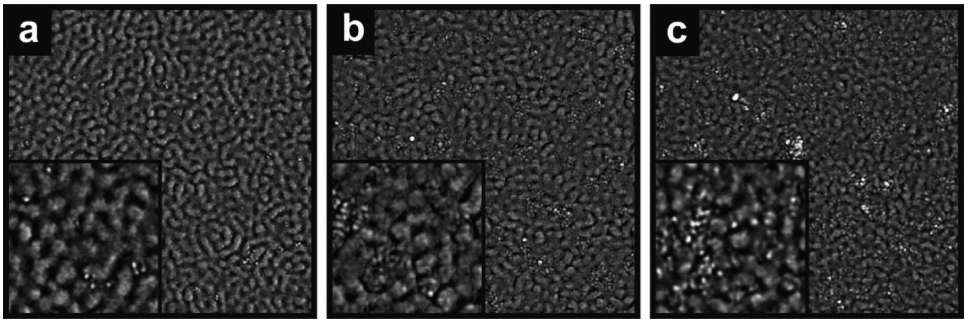

Figure 5. TM-AFM phase images (2 × 2 μm) of TiO_2/PS-*b*-PMMA nanocomposites containing (a) 1, (b) 3, and (c) 5 wt % of TiO_2 nanorods. The insets are images with higher magnification (0.5 × 0.5 μm).

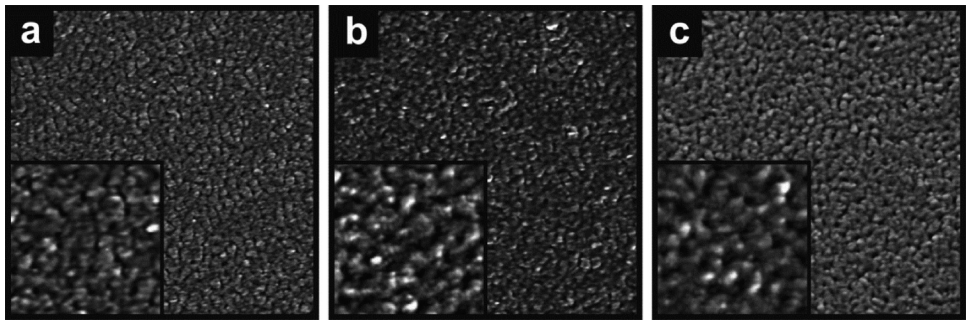

Figure 6. TM-AFM phase images (2 × 2 μm) of TiO_2/PS-*b*-PMMA nanocomposites containing (a) 10, (b) 15, and (c) 20 wt % of TiO_2 nanorods. The insets are images with higher magnification (0.5 × 0.5 μm).

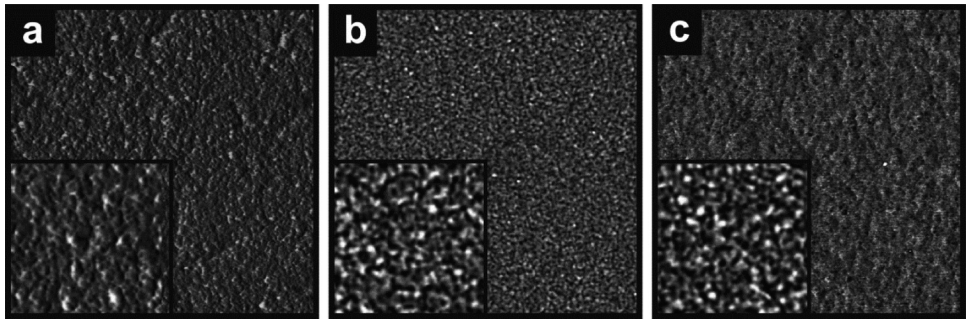

Figure 7. TM-AFM phase images (2 × 2 μm) of TiO_2/PS-*b*-PMMA nanocomposites containing (a) 30, (b) 40, and (c) 50 wt % of TiO_2 nanorods. The insets are images with higher magnification (0.5 × 0.5 μm).

brighter phase corresponding to the PMMA block, as can be observed in the inset of Figure 5a. Once again, the Hoftyzer and van Krevelen method[48] was used to calculate the Flory–Huggins interaction parameters between TiO_2 nanorods and each block of the block copolymer.[55,56] For this calculation, the nanorod capping layer consisting of oleic acid was taken into account. Therefore, the interaction parameter between PS block and oleic acid was 0.45, and the interaction parameter between PMMA block and oleic acid was 1.07, indicating that TiO_2 nanorods had a stronger affinity with the PS block than with the PMMA block due to the presence of the oleic acid layer covering the nanorod surface. This is in good agreement with AFM images, which showed a preferential location of TiO_2 nanorods in the PS block rich phase.

Figures 5b,c and 6a (3, 5, and 10 wt %) also show cylindrical morphologies with different sizes of the microseparated phase, which showed more closely packed cylindrical domains with an increase in TiO_2 nanorod content. For nanocomposite films containing 3 and 5 wt % of TiO_2 nanorods, only some dispersed nanorods or small nanorod aggregates appeared in the PS-*b*-PMMA matrix. Nevertheless, a cylindrical morphology of bright cylinders in a dark matrix was still present.

When nanorod content increased, the nanorods formed larger aggregates, resulting in a continuous bright matrix of the nanocomposite films with nanorod loading starting from 10 wt %. In the 10 wt % TiO_2/PS-*b*-PMMA nanocomposite film, the extent of the bright phase to almost all the film surface can be observed. Such a bright phase can be ascribed not only to the PMMA block but also to harder inorganic TiO_2 nanorods confined in the PS block of the diblock copolymer and preferably localized in this phase close to the interphase between blocks.[52−54] Therefore, the bright phase became predominant for this nanocomposite film and for nanocomposites with TiO_2 nanorod content higher than 10 wt %, preventing us from clearly discerning between PMMA rich phase and TiO_2/PS rich phase. Conversely, the small dark regions in the film can be safely ascribed to the PS block without TiO_2 nanorods.

Nanocomposite films at high TiO_2 nanorod content (higher than 10 wt %, Figures 6b,c and 7) showed completely different morphologies from those of films obtained with lower nanorod loading. Micrographs of these nanocomposite films showed a rather uniform and regular surface. However, in these cases, the typical block copolymer microphase separation, especially at high TiO_2 nanorod content, cannot be clearly discerned. Such evidence can be accounted for by the fact that PS block could be completely filled by TiO_2 nanorods, thus inducing a full TiO_2/PS phase coverage of the film surface and preventing the detection of PMMA block domains.[57] Nevertheless, PS-*b*-PMMA block copolymer apparently acts as a template for the TiO_2 nanorods, providing an overall regular surface containing uniformly dispersed TiO_2 nanorod assemblies.

Conductive properties of the prepared nanocomposite films composed of as-synthesized colloidal TiO_2 nanorods and PS-*b*-PMMA diblock copolymer were investigated by EFM. Different positive and negative voltages were applied to the EFM tip, and the different responses were analyzed. Here, the phase images corresponding to −6, 0, and 6 V voltages applied to surfaces of neat PS-*b*-PMMA block copolymer 3, 10, and 20 wt % TiO_2/PS-*b*-PMMA nanocomposites are reported (Figure 8). It should be mentioned that, remarkably, no sample showed any response when 0 V voltage was applied to the surface. Moreover, as expected, the surface of neat PS-*b*-PMMA block copolymer did not present any bright domain at any applied voltage, indicating that the block copolymer did not respond to the voltage and confirming that block copolymer is an uncharged material. Consequently, in TiO_2/PS-*b*-PMMA nanocomposites, the only conductive component could be

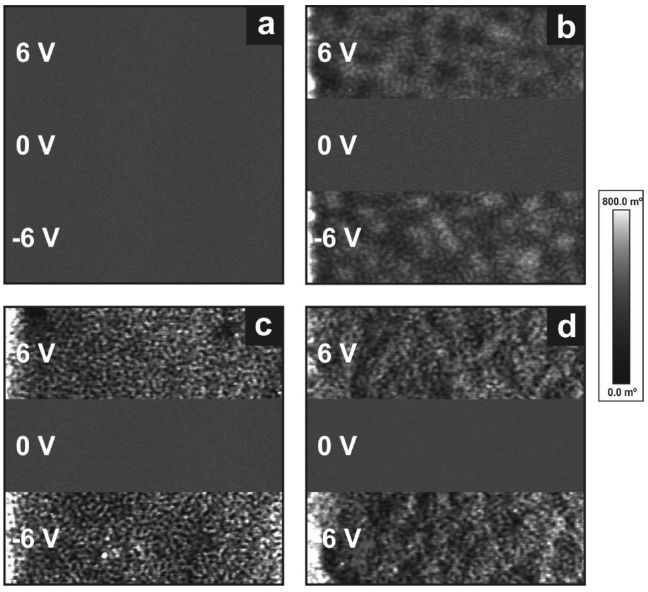

Figure 8. EFM phase images (3 × 3 μm) of (a) neat PS-*b*-PMMA block copolymer and (b) 3, (c) 10, and (d) 20 wt % TiO_2/PS-*b*-PMMA nanocomposites applying −6, 0, and 6 V.

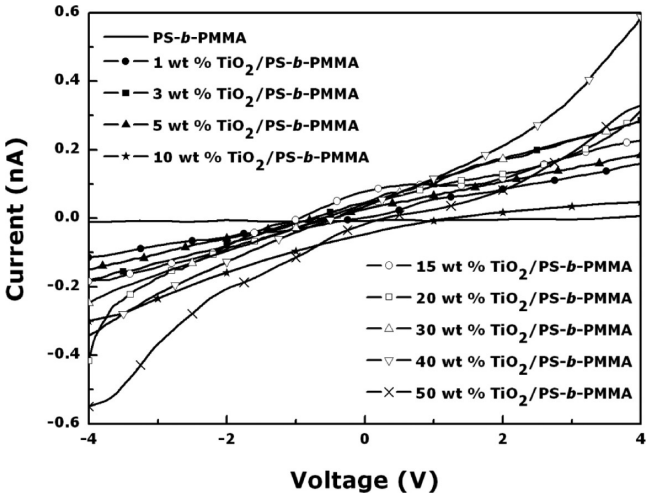

Figure 9. Current−voltage curves (I−V) for neat PS-*b*-PMMA block copolymer and 1, 3, 5, 10, 15, 20, 30, 40, and 50 wt % TiO_2/PS-*b*-PMMA nanocomposites applying a voltage sweep between −4 and 4 V.

TiO_2 nanorods.[24,29,34] In fact, when voltage values different from zero were applied, all nanocomposite samples showed a specific response dependent on the value of the applied voltage and the content of TiO_2 nanorods. In the cases of 3, 10, and 20 wt % TiO_2/PS-*b*-PMMA nanocomposite films, some bright domains appeared and showed a structure similar to that visible in the corresponding AFM images. The bright domains were indicative of the presence of a conductive material confined in such domains. In particular, these bright domains can be related to the presence of TiO_2 nanorods, which proves the nanorod confinement and the conductive character of the nanocomposite films. Furthermore, it can be seen that the intensity of the bright domains and the amount of bright conductive domains changed with the increase in the TiO_2 nanorod content in the nanocomposite films, thus confirming that the incorporation of the TiO_2 nanorods affected to the conductive behavior of the nanocomposite films.

Conductive properties at macroscale of fabricated TiO_2/PS-*b*-PMMA nanocomposites were measured with a Keithley semiconductor analyzer. Current−voltage curves (I−V) for each sample were recorded by applying a voltage sweep between −4 and 4 V. Figure 9 shows the current−voltage curves corresponding to all investigated samples. This analysis offers a qualitative tool to investigate the electrical response of prepared nanocomposites to the applied voltage. First, it can be seen that the curve of the neat PS-*b*-PMMA block copolymer appeared almost horizontal, confirming, as expected, no conductivity. On the contrary, all nanocomposites showed nonhorizontal curves, with a slight general trend of higher slope, and consequently higher intensity values for the voltage range, for higher TiO_2 nanorod content in the nanocomposites, especially for contents higher than 15 wt %. This indicates that TiO_2 nanorods are responsible for the conductive properties of the nanocomposites.[29,30,34] However, in spite of a slight trend, no significant difference can be observed as a function of nanorod content. This evidence could be because even for the highest TiO_2 nanorod content, 50 wt % of the nanocomposite was still composed of nonconductive PS-*b*-PMMA. Such results make these nanocomposite materials good potential candidates for semiconductor applications.

Taking into account the promising results obtained using EFM and the Keithley semiconductor analyzer, the quantitative conductive properties of the TiO_2/PS-*b*-PMMA nanocomposites with higher nanorod content were analyzed by atomic force microscopy in the PF-TUNA mode. The TUNA measurements allow us to investigate the conductivity of TiO_2 nanorods and TiO_2 based nanocomposites.[57−60] Images corresponding to 30, 40, and 50 wt % TiO_2/PS-*b*-PMMA nanocomposites are shown in Figure 10. Nanocomposite samples were then exposed to UV light for 24 h to degrade organic components in the nanocomposite films, including both block copolymer and nanorod organic ligand and thus obtaining TiO_2 nanorods based structures on the substrate.[23,61,62] These results are also reported in Figure 10d−f. All images exhibit the TUNA current map when applying voltages of −6, 0, and 6 V. Additionally, the current profiles corresponding to a horizontal section of the images of −6 and 6 V are included to give more detailed information about current values passing through the investigated samples.

When a voltage of 0 V was applied, no current was detected in any of the samples, as expected. In the case of non-UV-treated samples (Figure 10a−c), the images obtained after applying a positive voltage of 6 V showed mainly the same absence of current as observed in the case of 0 V applied, whereas when a negative voltage of −6 V was applied, some dark spheres appeared in the images, indicating a current response. In general, these three analyzed samples presented a current near zero and a dark surface when a positive voltage was applied and, conversely, a current up to −1.2 pA and some almost black spheres when a negative voltage was applied. This evidence indicates that the application of negative voltage has a stronger influence on the conductive behavior of the colloidal TiO_2 nanorods, as also observed in the resulting data from semiconductor analyzer measurements. Differences in the responses to positive or negative voltages have been previously reported in literature.[61] In addition, the 30 wt % TiO_2/PS-*b*-PMMA nanocomposite presented higher current values passing throughout the sample and a more regular distribution of the local currents on the whole surface in comparison to

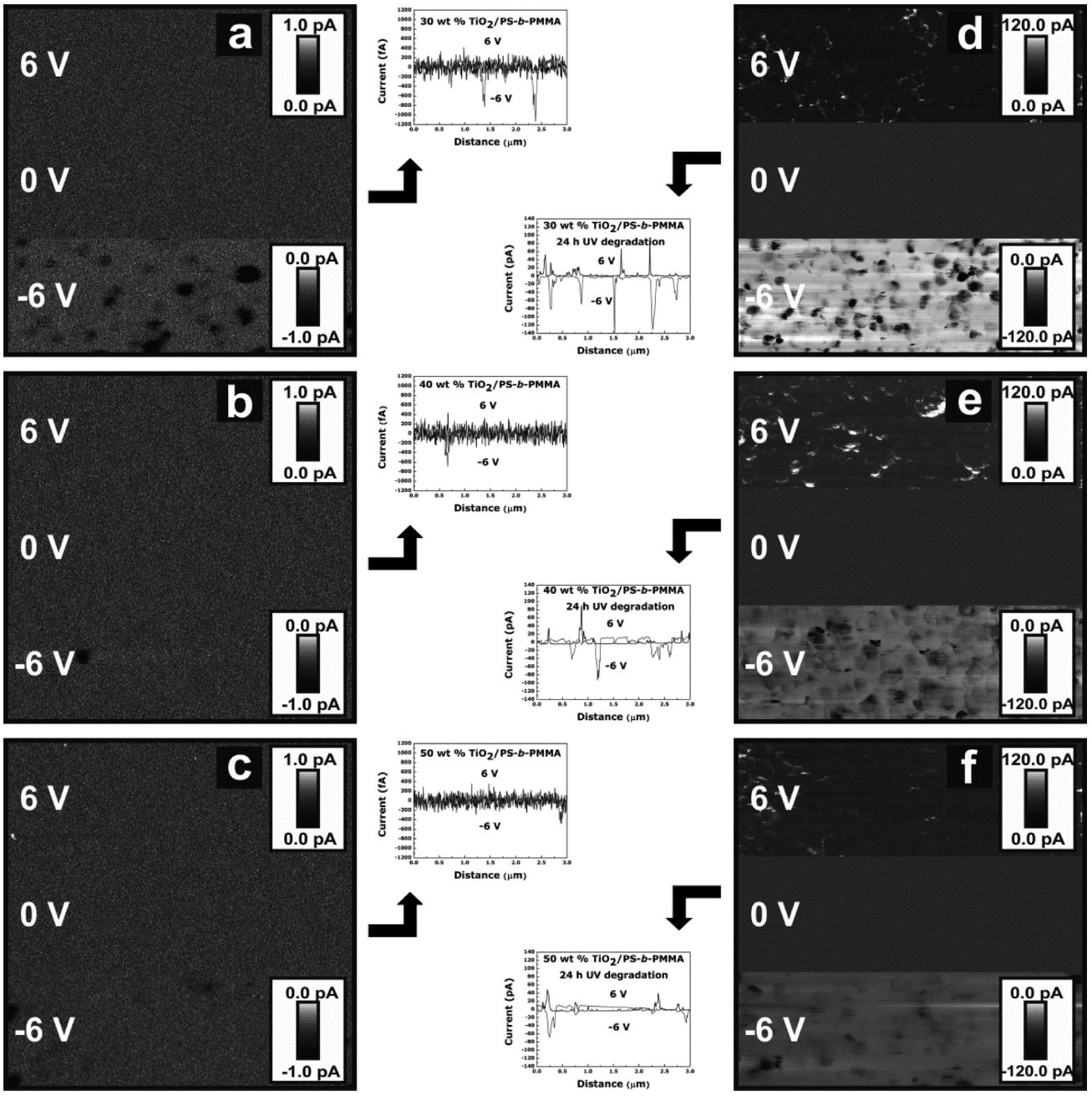

Figure 10. TUNA current images (3 × 3 μm) taken at voltages of −6, 0, and 6 V for (a) 30, (b) 40, and (c) 50 wt % TiO_2/PS-*b*-PMMA nanocomposites and for (d) 30, (e) 40, and (f) 50 wt % TiO_2/PS-*b*-PMMA after being exposed to UV light for 24 h. The graphs correspond to horizontal section profiles of each −6 and 6 V images.

nanocomposites with 40 and 50 wt % TiO_2 nanorod contents, which only displayed isolated local currents in whole sample. The 50 wt % TiO_2/PS-*b*-PMMA sample image exhibited some small white dots in the image, corresponding to the positive bias, which could be related to the presence of the semiconductive TiO_2 nanorods. Taking into account the profiles obtained from the current maps, it can be clearly seen that, generally, the response to inverse bias is higher, as observed in the images. The 30 wt % TiO_2/PS-*b*-PMMA nanocomposite reached the highest current values, approximately up to −1.2 pA, whereas 40 and 50 wt % TiO_2/PS-*b*-PMMA nanocomposites had lower values, up to −0.7 and −0.4, respectively, and also more isolated local currents. Such current values are in the same order of magnitude of the values obtained in previous works for polymeric nanocomposites modified with TiO_2 nanoparticles.[57]

However, the current does not follow a clear trend with nanorod loading. This result can be explained considering that even at a higher nanoparticle content in the nanocomposite, in the analyzed surface, nanorods were embedded in the block copolymer block, which is nonconductive and therefore did not allow full electrical contact among the nanostructures through the sample, thus affecting the significance of the current measurements as a function of nanorod loading.

However, as can be observed from the comparison between panels a−c and panels d−f in Figure 10, the exposure to UV light of the samples caused a significant change in the TUNA current passing throughout the samples when both direct and

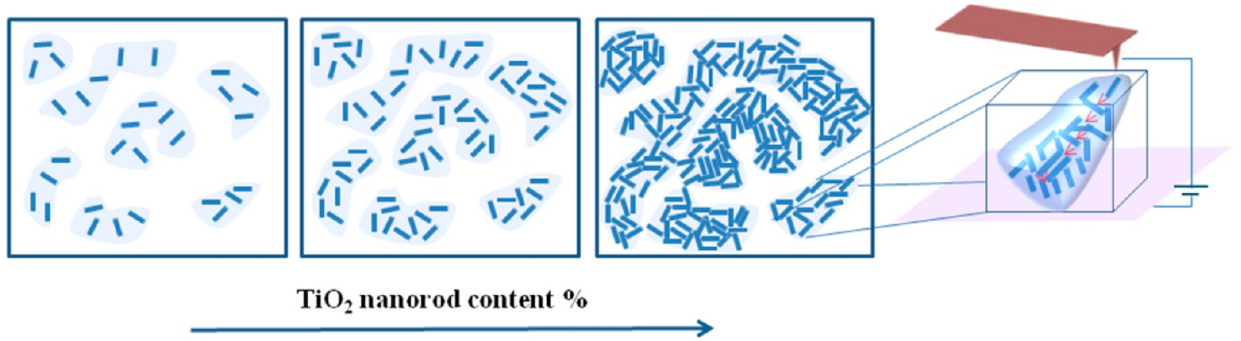

Figure 11. Schematic representation of the conductive behavior of the TiO_2/PS-*b*-PMMA nanocomposite films varying the TiO_2 nanorod content.

inverse voltages were applied. This phenomenon could be explained by taking into account that the exposure to UV light led to the degradation of the organic components of the nanocomposites and consequently to the investigation of the surface covered by TiO_2 nanorod based structures. Nanocomposites containing 30, 40, and 50 wt % TiO_2 nanorods treated with UV light showed considerably higher TUNA currents (Figure 10d–f) in comparison to the same 30, 40, and 50 wt % TiO_2/PS-*b*-PMMA samples before their exposure to UV light. As a result of degradation of the organic components of the nanocomposites, the measured current increased, indicating more conductive surfaces. This evidence is consistent with the reported consideration that TiO_2 nanorods are the only component in the nanocomposite with a conductive behavior.[24,29,34] Therefore, degradation of the organic components enhanced the conductive properties of these films. In the case of the nanocomposites treated with UV light, when 0 V were applied, no response was detected in the surfaces, similar to the untreated samples. However, TUNA currents can be seen in the images of 30, 40, and 50 wt % TiO_2/PS-*b*-PMMA nanocomposites with the application of both direct and inverse bias. It should be taken into account that even if the scale bars of positive and negative voltages are the same, the corresponding profiles indicated that, once again, the responses to negative voltage were greater. From these profiles, we could determine the highest TUNA currents of these samples. With the application of 6 V, around 80, 90, and 50 pA were reached for the 30, 40, and 50 wt % of TiO_2 nanorod contents, respectively, and for the −6 V bias, around −140, −90, and −70 pA, respectively, for the same nanocomposites. Comparing the three investigated nanocomposite films, in the case of the positive voltage, the white areas of the surface became brighter with the addition of 40 wt % and less evident with the addition of 50 wt % TiO_2 nanorods. Additionally, the darker area of these images also became slightly clearer at higher nanorod content. On the other hand, the dark spots corresponding to the inverse voltage were fewer and less intense in the cases of 40 and 50 wt % TiO_2 nanorods, whereas the background of the images was darker with increased nanorod content. Then at higher amount of TiO_2 nanorods, after UV treatment, the local detected current is lower, but the darker background suggests that the whole surface is more conductive. This finding can be explained taking into account that after UV treatment, charge percolation paths formed through the sample, thus leading to high currents. The schematic representation in Figure 11 helps to visualize this behavior. After UV treatment, a clear dependence of the conductivity on the nanorod content was found, as a more conductive film was obtained at higher nanorod loading.

CONCLUSIONS

In summary, nanocomposites with high optical and conductive properties were obtained by incorporating as-synthesized colloidal TiO_2 nanorods into the self-assembled PS-*b*-PMMA diblock copolymer. The optical properties of the nanocomposite solutions were confirmed by the UV–vis absorption behavior shown by all samples.

The TiO_2 nanorod capping layer consisting of oleic acid molecules enabled us to disperse a high content of TiO_2 nanorods in the nanocomposites, up to 50 wt % with respect to the block copolymer content. TiO_2/PS-*b*-PMMA nanocomposites with low contents of TiO_2 nanorods presented a clear cylindrical morphology as confirmed by AFM; however, when the content of TiO_2 nanorods increased, the presence of high nanorod quantity hindered the detection of the typical morphologies attributed to block copolymers. TiO_2 nanorods had a stronger affinity with the PS block of the block copolymer, and consequently, they were located mainly in that phase, changing the ratio between blocks upon the addition of nanoparticles. When TiO_2 nanorod content higher than 30 wt % content was added to the block copolymer, the extended coverage of TiO_2 nanorods on the sample surface was achieved.

In addition, EFM results indicated that domains where TiO_2 nanorods were located, namely the TiO_2/PS rich phase, were conductive, whereas the PMMA rich phase did not show any conductivity. In addition, PeakForce TUNA results proved high conductivity of nanocomposites with 30, 40, and 50 wt % of TiO_2 nanorods, when the organic component of the film was removed by exposure to UV light, leaving TiO_2 nanorods based structures. Such evidence can be explained by the occurrence of percolation paths through the nanorod based assembly in the sample. Additionally, the conductive properties at macroscale, studied by applying a sweep voltage, were dependent on TiO_2 nanorod loading.

The optical and semiconductive properties of the TiO_2 nanorod based nanocomposites, along with the opportunity offered by the block copolymer of fabricating TiO_2 based structures, open the venue to the integration of such functional nanostructured materials for applications in memory and optoelectronic devices, catalysts, and sensors, as well as in energy conversion fields.

AUTHOR INFORMATION

Corresponding Author

*Tel.: +34 943 017 163. Fax: +34 943 017 130. E-mail: agnieszka.tercjaks@ehu.es.

Notes

The authors declare no competing financial interest.

■ ACKNOWLEDGMENTS

This work was supported by the EU-funded Seventh Framework Programme project LIMPID (Grant 310177), by MAAT PON project (CUPB31C12001230005, "Molecular Nanotechnology for Health and Environment"), by the Spanish Ministry of Economy and Competitiveness funded project (MAT2012-31675), and by the Basque Government funded Grupos Consolidados project (IT776-13). L.C. thanks Eusko Jaurlaritza/Gobierno Vasco for the Ph.D. fellowship (Programas de Becas para Formación y Perfeccionamiento de Personal Investigador (PRE_2013_2_418)). A.T. acknowledges MICINN for Ramón y Cajal program (RYC-2010-05592). Moreover, we are grateful to the 'Macrobehavior−Mesostructure−Nanotechnology' SGIker unit of the UPV/EHU.

■ REFERENCES

(1) Jang, B. N.; Wang, D.; Wilkie, C. A. Relationship between the Solubility Parameter of Polymers and the Clay Dispersion in Polymer/Clay Nanocomposites and the Role of the Surfactant. *Macromolecules* **2005**, *38*, 6533−6543.

(2) Hussain, F.; Hojjati, M.; Okamoto, M.; Gorga, R. E. Review article: Polymer-Matrix Nanocomposites, Processing, Manufacturing, and Application: An Overview. *J. Compos. Mater.* **2006**, *14*, 1511−1575.

(3) Cipriari, D.; Jacob, K.; Tannenbaum, R. Characterization of Polymer Nanocomposite Interphase and Its Impact on Mechanical Properties. *Macromolecules* **2006**, *39*, 6565−6573.

(4) Cui, F.; Liang, S.; Zhang, J.; Han, Y.; Lü, C.; Cui, T.; Yang, B. Formation of Nanoparticles in Solid-State Matrices: A Strategy for Bulk Transparent TiO_2-Polymer Nanocomposites. *Polym. Chem.* **2012**, *3*, 3296−3300.

(5) Kim, D.; Srivastava, S.; Narayanan, S.; Archer, L. A. Polymer Nanocomposites: Polymer and Particle Dynamics. *Soft Matter* **2012**, *8*, 10813−10818.

(6) Mutz, M.; Holley, D. W.; Baskaran, D.; Mays, J. W.; Dadmun, M. D. Impact of Nanoparticle Size and Shape on Selective Surface Segregation in Polymer Nanocomposites. *Polymer* **2012**, *53*, 5087−5096.

(7) Nardi, T.; Sangermano, M.; Leterrier, Y.; Allia, P.; Tiberto, P.; Manson, J. A. E. UV-Cured Transparent Magnetic Polymer Nanocomposites. *Polymer* **2013**, *54*, 4472−4479.

(8) Schmidt, G.; Malwitz, M. M. Properties of Polymer-Nanoparticle Composites. *Curr. Opin. Colloid Interface Sci.* **2003**, *8*, 103−108.

(9) Dutta, K.; De, S. K. Electrical Conductivity and Dielectric Properties of SiO_2 Nanoparticles Dispersed in Conducting Polymer Matrix. *J. Nanopart. Res.* **2007**, *9*, 631−638.

(10) Fung, D. D. S.; Qiao, L.; Choy, W. C. H.; Wang, C.; Sha, W. E. I.; Xie, F.; He, S. Optical and Electrical Properties of Efficiency Enhanced Polymer Solar Cells with Au Nanoparticles in a PEDOT-PSS Layer. *J. Mater. Chem.* **2011**, *21*, 16349−16356.

(11) Cho, M. S.; Park, S. Y.; Hwang, J. Y.; Choi, H. J. Synthesis and Electrical Properties of Polymer Composites with Polyaniline Nanoparticles. *Mater. Sci. Eng., C* **2004**, *24*, 15−18.

(12) Kim, S. H.; Misner, M. J.; Xu, T.; Kimura, M.; Russell, T. P. Highly Oriented and Ordered Arrays from Block Copolymers via Solvent Evaporation. *Adv. Mater.* **2004**, *16*, 226−231.

(13) Metwalli, E.; Perlich, J.; Wang, W.; Diethert, A.; Roth, S. V.; Papadakis, C. M.; Müller-Buschbaum, P. Morphology of Semicrystalline Diblock Copolymer Thin Films upon Directional Solvent Vapor Flow. *Macromol. Chem. Phys.* **2010**, *211*, 2102−2108.

(14) Deng, T.; Chen, C.; Honeker, C.; Thomas, E. L. Two-Dimensional Block Copolymer Photonic Crystals. *Polymer* **2003**, *44*, 6549−6553.

(15) Angelescu, D. E.; Waller, J. H.; Register, R. A.; Chaikin, P. M. *Adv. Mater.* **2005**, *17*, 1878−1881.

(16) Böker, A.; Elbs, H.; Hänsel, H.; Knoll, A.; Ludwigs, S.; Zettl, H.; Zvelindovsky, A. V.; Sevink, G. J. A.; Urban, V.; Abetz, V.; Müller, A. H. E.; Krausch, G. *Macromolecules* **2003**, *36*, 8078−8087.

(17) Hamley, I. W. Nanostructure Fabrication Using Block Copolymers. *Nanotechnology* **2003**, *14*, 39−54.

(18) Haryono, A.; Binder, W. H. Controlled Arrangement of Nanoparticle Arrays in Block-Copolymer Domains. *Small* **2006**, *2*, 600−611.

(19) Bockstaller, M. R.; Mickiewicz, R. A.; Thomas, E. L. Block Copolymer Nanocomposites: Perspectives for Tailored Functional Materials. *Adv. Mater.* **2005**, *17*, 1331−1349.

(20) Chiu, J. J.; Kim, B. J.; Kramer, E. J.; Pine, D. J. Control of Nanoparticle Location in Block Copolymers. *J. Am. Chem. Soc.* **2005**, *127*, 5036−5037.

(21) Luo, M.; Epps, T. H. Directed Block Copolymer Thin Film Self-Assembly: Emerging Trends in Nanopattern Fabrication. *Macromolecules* **2013**, *46*, 7567−7579.

(22) Binder, W. H.; Kluger, C.; Straif, C. J.; Friedbacher, G. Directed Nanoparticle Binding onto Microphase-Separated Block Copolymer Thin Films. *Macromolecules* **2005**, *38*, 9405−9410.

(23) Thurn-Albrecht, T.; Steiner, R.; DeRouchey, J.; Stafford, C. M.; Huang, E.; Bal, M.; Tuominen, M.; Hawker, C. J.; Russell, T. P. Nanoscopic Templates from Oriented Block Copolymer Films. *Adv. Mater.* **2000**, *12*, 787−791.

(24) Pan, J. H.; Zhao, X. S.; Lee, W. I. Block Copolymer-Templated Synthesis of Highly Organized Mesoporous TiO_2-Based Films and Their Photoelectrochemical Applications. *Chem. Eng. J.* **2011**, *170*, 363−380.

(25) Burda, C.; Lou, Y.; Chen, X.; Samia, A. C. S.; Stout, J.; Gole, J. L. Enhanced Nitrogen Doping in TiO_2 Nanoparticles. *Nano Lett.* **2003**, *3*, 1049−1051.

(26) Weng, C. C.; Wei, K. H. Selective Distribution of Surface-Modified TiO_2 Nanoparticles in Polystyrene-b-poly(methyl methacrylate) Diblock Copolymer. *Chem. Mater.* **2003**, *15*, 2936−2941.

(27) Sun, Z.; Kim, D. H.; Wolkenhauer, M.; Bumbu, G. G.; Knoll, W.; Gutmann, J. S. Synthesis and Photoluminescence of Titania Nanoparticle Arrays Templated by Block-Copolymer Thin Films. *ChemPhysChem* **2006**, *7*, 370−378.

(28) Gutierrez, J.; Tercjak, A.; Garcia, I.; Peponi, L.; Mondragon, I. Hybrid Titanium Dioxide/PS-b-PEO Block Copolymer Nanocomposites Based on Sol−Gel Synthesis. *Nanotechnology* **2008**, *19*, 155607.

(29) Gutierrez, J.; Tercjak, A.; Peponi, L.; Mondragon, I. Conductive Properties of Inorganic and Organic TiO_2/Polystyrene-block-poly(ethylene oxide) Nanocomposites. *J. Phys. Chem. C* **2009**, *113*, 8601−8605.

(30) Yen, W. C.; Lee, Y. H.; Lin, J. F.; Dai, C. A.; Jeng, U. S.; Su, W. F. Effect of TiO_2 Nanoparticles on Self-Assembly Behaviors and Optical and Photovoltaic Properties of the P3HT-b-P2VP Block Copolymer. *Langmuir* **2011**, *27*, 109−115.

(31) Scalarone, D.; Tata, J.; Caldera, F.; Lazzari, M.; Chiantore, O. Porous and Worm-like Titanium Dioxide Nanostructures from PS-b-PEO Block Copolymer Micellar Solutions. *Mater. Chem. Phys.* **2011**, *128*, 166−171.

(32) Gurevitch, I.; Buonsanti, R.; Teran, A. A.; Gludovatz, B.; Ritchie, R. O.; Cabana, J.; Balsara, N. P. Nanocomposites of Titanium Dioxide and Polystyrene-poly(ethylene oxide) Block Copolymer as Solid-State Electrolytes for Lithium Metal Batteries. *J. Electrochem. Soc.* **2013**, *160*, A1611−A1617.

(33) Xiao, J.; Chen, W.; Wang, F.; Du, J. Polymer/TiO_2 Hybrid Nanoparticles with Highly Effective UV-Screening but Eliminated Photocatalytic Activity. *Macromolecules* **2013**, *46*, 375−383.

(34) Cano, L.; Gutierrez, J.; Tercjak, A. Rutile TiO_2 Nanoparticles Dispersed in a Self-Assembled Polystyrene-block-polymethyl Methacrylate Diblock Copolymer Template. *J. Phys. Chem. C* **2013**, *117*, 1151−1156.

(35) Convertino, A.; Leo, G.; Striccoli, M.; Di Marco, G.; Curri, M. L. Effect of Shape and Surface Chemistry of TiO_2 Colloidal Nanocrystals on the Organic Vapor Absorption Capacity of TiO_2/PMMA Composite. *Polymer* **2008**, *49*, 5526−5532.

(36) Sciancalepore, C.; Cassano, T.; Curri, M. L.; Mecerreyes, D.; Valentini, A.; Agostiano, A.; Tommasi, R.; Striccoli, M. TiO_2 Nanorods/PMMA Copolymer-Based Nanocomposites: Highly Homogeneous Linear and Nonlinear Optical Material. *Nanotechnology* **2008**, *19*, 205705.
(37) Petronella, F.; Fanizza, E.; Mascolo, G.; Locaputo, V.; Bertinetti, L.; Martra, G.; Coluccia, S.; Agostiano, A.; Curri, M. L.; Comparelli, R. Photocatalytic Activity of Nanocomposite Catalyst Films Based on Nanocrystalline Metal/Semiconductors. *J. Phys. Chem. C* **2011**, *115*, 12033−12040.
(38) Convertino, A.; Tamborra, M.; Striccoli, M.; Leo, G.; Agostiano, A.; Curri, M. L. Poly(methyl methacrylate) Nanocomposites Based on TiO_2 Nanocrystals: Tailoring Material Properties Towards Sensing. *Thin Solid Films* **2011**, *519*, 3931−3938.
(39) Cozzoli, P. D.; Kornowski, A.; Weller, H. Low-Temperature Synthesis of Soluble and Processable Organic-Capped Anatase TiO_2 Nanorods. *J. Am. Chem. Soc.* **2003**, *125*, 14539−14548.
(40) Fanizza, E.; Cozzoli, P. D.; Curri, M. L.; Striccoli, M.; Sardella, E.; Agostiano, A. UV-Light-Driven Immobilization of Surface-Functionalized Oxide Nanocrystals onto Silicon. *Adv. Funct. Mater.* **2007**, *17*, 201−211.
(41) Gutierrez, J.; Tercjak, A.; Garcia, I.; Mondragon, I. The Effect of Thermal and Vapor Annealing Treatments on the Self-Assembly of TiO_2/PS-b-PMMA Nanocomposites Generated Via the Sol-Gel Process. *Nanotechnology* **2009**, *20*, 225603.
(42) Meng, X.; Zhang, Z.; Luo, N.; Cao, S.; Yang, M. Transparent Poly(methyl methacrylate)/TiO_2 Nanocomposites for UV-Shielding Applications. *Polym. Sci., Ser. A* **2011**, *53*, 977−983.
(43) Tercjak, A.; Gutierrez, J.; Martin, M. D.; Mondragon, I. Transparent Titanium Dioxide/Block Copolymer Modified Epoxy-Based Systems in the Long Scale Microphase Separation Threshold. *Eur. Polym. J.* **2012**, *48*, 16−25.
(44) Lee, H. S.; Koo, S. M.; Yoo, J. W. TiO_2-SiO_2 Nanoparticles for Suppressing Photocatalytic Activities and Improving Hydrophilicity. *J. Ceram. Process. Res.* **2012**, *13*, 300−303.
(45) Lopes, W. A.; Jaeger, H. M. Hierarchical Self-Assembly of Metal Nanostructures on Diblock Copolymer Scaffolds. *Nature* **2001**, *414*, 735−738.
(46) Ham, S.; Shin, C.; Kim, E.; Ryu, D. Y.; Jeong, U.; Russel, T. P.; Hawker, C. J. Microdomain Orientation of PS-b-PMMA by Controlled Interfacial Interactions. *Macromolecules* **2008**, *41*, 6431−6437.
(47) Yang, P.; Wang, S.; Teng, X.; Wei, W.; Dravid, V. P.; Huang, L. Effect of Magnetic Nanoparticles on the Morphology of Polystyrene-b-poly(methyl methacrylate) Diblock Copolymer Thin Film. *J. Phys. Chem. C* **2012**, *116*, 23036−23040.
(48) Kim, E.; Ahn, H.; Park, S.; Lee, H.; Lee, M.; Lee, S.; Kim, T.; Kwak, E.; Lee, J. H.; Lei, X.; Huh, J.; Bang, J.; Lee, B.; Ryu, D. Y. Directed Assembly of High Molecular Weight Block Copolymers: Highly Ordered Line Patterns of Perpendicularly Oriented Lamellae with Large Periods. *ACS Nano* **2013**, *7*, 1952−1960.
(49) Van Krevelen, D. W. *Properties of Polymers*, 4th ed.; Elsevier Science B.V.: Amsterdam, 1990; pp 213−216.
(50) Xuan, Y.; Peng, J.; Cui, L.; Wang, H.; Li, B.; Han, Y. Morphology Development of Ultrathin Symmetric Diblock Copolymer Film via Solvent Vapor Treatment. *Macromolecules* **2004**, *37*, 7301−7307.
(51) Venugopal, G.; Krause, S. Development of Phase Morphologies of Poly(methyl methacrylate)-Polystyrene-Toluene Mixtures in Electric Fields. *Macromolecules* **1992**, *25*, 4626−4634.
(52) Tercjak, A.; Gutierrez, J.; Peponi, L.; Rueda, L.; Mondragon, I. Arrangement of Conductive TiO_2 Nanoparticles in Hybrid Inorganic/Organic Thermosetting Materials Using Liquid Crystal. *Macromolecules* **2009**, *42*, 3386−3390.
(53) Lamarre, S. S.; Lemay, C.; Labrecque, C.; Ritcey, A. M. Controlled 2D Organization of Gold Nanoparticles in Block Copolymer Monolayers. *Langmuir* **2013**, *29*, 10891−10898.
(54) Di Mauro, A. E.; Striccoli, M.; Depalo, N.; Fanizza, E.; Cano, L.; Ingrosso, C.; Agostiano, A.; Curri, M. L.; Tercjak, A. Selective Confinement of Oleylamine Capped Au Nanoparticles in Self-Assembled PS-b-PEO Diblock Copolymer Templates. *Soft Matter* **2014**, *10*, 1676−1684.
(55) Rawolle, M.; Braden, E. V.; Niedermeier, M. A.; Magerl, D.; Sarkar, K.; Fröschl, T.; Hüsing, N.; Perlich, J.; Müller-Buschbaum, P. Low-Temperature Route to Crystalline Titania Network Structures in Thin Films. *ChemPhysChem* **2012**, *13*, 2412−2417.
(56) Perlich, J.; Memesa, M.; Diethert, A.; Metwalli, E.; Wang, W.; Roth, S. V.; Gutmann, J. S.; Müller-Buschbaum, P. Layer-by-layer Fabrication of an Anatase Titania Multilayer with Gradual Sponge-like Morphology. *Colloid Polym. Sci.* **2012**, *290*, 119−126.
(57) Gutierrez, J.; Tercjak, A.; Mondragon, I. Conductive Behavior of High TiO_2 Nanoparticle Content of Inorganic/Organic Nanostructured Composites. *J. Am. Chem. Soc.* **2010**, *132*, 873−878.
(58) Prastani, C.; Vetushka, A.; Fejfar, A.; Nanu, M.; Nanu, D.; Rath, J. K.; Schropp, R. E. I. Conductivity Mapping of Nanoparticles by Torsional Resonance Tunneling Atomic Force Microscopy. *Appl. Phys. Lett.* **2012**, *101*, 083107.
(59) Tercjak, A.; Gutierrez, J.; Ocando, C.; Mondragon, I. Conductive Properties of Switchable Photoluminescence Thermosetting Systems Based on Liquid Crystals. *Langmuir* **2010**, *26*, 4296−4302.
(60) Gutierrez, J.; Mondragon, I.; Tercjak, A. Quantitative Nanoelectrical and Nanomechanical Properties of Nanostructured Hybrid Composites by PeakForce Tunneling Atomic Force Microscopy. *J. Phys. Chem. C* **2014**, *118*, 1206−1212.
(61) Hsueh, H. Y.; Chen, H. Y.; She, M. S.; Chen, C. K.; Ho, R. M.; Gwo, S.; Hasegawa, H.; Thomas, E. L. Inorganic Gyroid with Exceptionally Low Refractive Index from Block Copolymer Templating. *Nano Lett.* **2010**, *10*, 4994−5000.
(62) Hsueh, H. Y.; Ho, R. M. Bicontinuous Ceramics with High Surface Area from Block Copolymer Templates. *Langmuir* **2012**, *28*, 8518−8529.